Journal of Sustainability, Policy, and Practice
EISSN: 3105-1448 | PISSN: 3105-143X | Vol. 1, No. 4 (2025)

Article

Effectiveness Evaluation of Adaptive Difficulty Adjustment Algorithms with Multimodal Feedback for Social Skills Training in Children with Autism Spectrum Disorder

Yaqing Bai [1,*]

[1] Human Development, University of Rochester, NY, USA
* Correspondence: Yaqing Bai; Human Development, University of Rochester, NY, USA

Abstract: Children diagnosed with autism spectrum disorder display substantial heterogeneity in social communication skills, necessitating intervention strategies that dynamically adapt to individual developmental trajectories. We propose a hierarchical reinforcement learning framework that integrates multimodal behavioral streams to guide difficulty progression in therapeutic social scenarios. Skill development is modeled as a constrained Markov decision process, with difficulty vectors d in D evolving according to composite performance signals p(t) and engagement indicators e(t), where the optimization objective J = E [sum over t of gamma ^ t * (r_skill (s_t, a_t) + lambda * r_engage (s_t, a_t))] balances immediate skill gains against sustained participation. Three synchronized channels-facial landmarks tracked via 68-point models sampled at 120 Hz, acoustic features represented by 13-dimensional MFCCs, and skeletal configurations captured across 25 anatomical joints-are processed through temporal convolutional networks. Attention-weighted aggregation f_fusion = sum over i of alpha_i * phi_i (x_i) allows each modality-specific encoder phi_i to contribute proportionally to its instantaneous reliability. Clinical trials involving 124 participants (ages 6-14, ADOS-2 scores 12.4 ± 3.2) demonstrate a 42.3% acceleration in competency acquisition compared with therapist-directed baselines (hierarchical model coefficient beta_time×condition = 1.42, SE = 0.18, t (1984) = 7.89, p < 0.001). Transition prediction between difficulty states achieves 87.4% accuracy. Power-law retention analysis indicates reduced forgetting in the adaptive framework (b_adaptive = 0.084 versus b_control = 0.162), with 78.4% of acquired competencies maintained at a 12-week follow-up.

Keywords: autism interventions; reinforcement learning architectures; behavioral signal processing; adaptive training systems; multimodal fusion

Received: 30 September 2025
Revised: 15 October 2025
Accepted: 07 November 2025
Published: 15 November 2025

1. Introduction

1.1. Clinical Landscape and Computational Opportunities

Neurodevelopmental divergence characteristic of autism spectrum conditions affects approximately one in forty-four children, although prevalence estimates vary with evolving diagnostic practices. Manifestations encompass disruptions in social reciprocity, communication asymmetries, and behavioral rigidity, with each dimension showing substantial variability within the diagnosis. Conventional therapeutic protocols typically prescribe predetermined sequences of difficulty. Such rigid scaffolding conflicts with observed heterogeneity in acquisition trajectories. Some children achieve rapid initial mastery followed by plateaus, whereas others require extended foundational support before progressing. Previous studies demonstrated engagement amplification up to 73%

when virtual reality platforms modulated environmental complexity responsively, indicating that technology-mediated individualization can be effective [1].

Optimal challenge calibration requires balancing frustration and boredom. This can be formalized as $Z_{pd} = \{d: P(\text{success} \mid d, \theta_i) \in [0.6, 0.8]\}$, defining the zone where capability parameters θ_i interact productively with difficulty d. Success probabilities below 60% lead to repeated failures that erode motivation, whereas probabilities above 80% provide insufficient cognitive challenge, limiting learning. Workforce constraints further complicate intervention delivery, as specialized practitioners can reach fewer than one-third of diagnosed populations. Geographic disparities exacerbate access inequities, with rural communities facing particular shortages.

Computational approaches offer the ability to transform episodic clinical observations into continuous optimization landscapes. Moment-to-moment behavioral signals enable real-time recalibration that is unattainable through human observation alone. However, key questions remain: Can algorithmic orchestration of difficulty parameters match the performance of experienced therapists? Beyond accuracy metrics, can automated systems sustain engagement, promote generalization, and ensure retention comparable to human-guided interventions?

1.2. Architectural Shortcomings in Contemporary Systems

Existing adaptive mechanisms often rely on simplistic threshold logic, expressed as $d_{t+1} = d_t + \gamma \cdot \text{sign}(p_t - p_{target})$. These formulations assume linear relationships between difficulty and performance. In practice, the interactions are more complex: cognitive demands multiply with sensory load, and emotional regulation influences all dimensions. Studies report that structured adaptation can improve peer interactions by 65%, yet multidimensional complexity remains insufficiently addressed [2].

Measurement challenges further hinder algorithmic adaptation. High discontinuation rates-up to 40% in vocabulary interventions reflect difficulties caused by misalignment between task demands and participant capabilities. Single-modality assessments correlate weakly ($r = 0.62$) with comprehensive evaluations. Attention fluctuates, anxiety varies, and sensory sensitivities change unpredictably. Observation noise, represented by σ^2_{obs}, necessitates probabilistic reasoning to maintain uncertainty bounds throughout adaptation cycles [3].

Learning trajectories are often non-linear. Breakthrough moments punctuate extended plateaus, and skills may temporarily regress before consolidating. Current frameworks lack mechanisms to accommodate such non-monotonic progression. Moreover, distinguishing between performance limitations due to capability versus fatigue remains unresolved. Inappropriate recalibrations can exacerbate rather than resolve learning obstacles.

2. Related Work and Theoretical Framework

2.1. Educational Optimization Through Reinforcement Learning

Sequential decision frameworks frame pedagogical adaptation as navigation through state-action spaces toward long-term objectives. States encode observable metrics augmented with latent constructs, while actions modify environmental parameters. Reward functions balance competing goals. Previous work demonstrated 52% improvement in generalization when multimodal architectures calibrated difficulty responsively. Their composite reward, $r_{total} = r_{skill} + \lambda_1 * r_{engage} - \lambda_2 * r_{cognitive\_load}$, balances skill demonstration against sustained participation while penalizing excessive cognitive demands [4].

Autism-specific adaptations expand conventional state representations. Beyond performance p_t, the augmented state vector $s_t = [p_t, \Delta p_t, e_t, h_t, c_t, \sigma_t]$ incorporates performance derivatives, engagement histories, emotional indicators, contextual moderators, and uncertainty quantification. This enables differentiation between genuine improvement and transient fluctuations. Constraints on modification

magnitudes Δd_max prevent abrupt transitions that could trigger dysregulation, which is especially relevant given the sensory sensitivities prevalent in autism populations.

Domain knowledge informs reward shaping through potential functions, preserving policy invariance. Curricula structure challenge sequences progressively, with mastery probabilities P (mastery | history) exceeding a threshold tau_mastery gating advancement. Rigid curricula, however, are suboptimal for heterogeneous learners. Adaptive sequencing must balance structure with flexibility.

2.2. Heterogeneous Signal Integration Architectures

Behavioral manifestations span multiple modalities operating at different frequencies and varying reliability. Studies revealed that reinforcement learning signatures can be traced through synchronized neural and behavioral recordings, uncovering reward processing components specific to autism. Observable actions interact with hidden cognitive processes, necessitating multimodal inference [5].

Virtual reality studies achieved 81% precision in predicting prompt timing by fusing gaze dynamics sampled at 250 Hz, gestural patterns at 30 Hz, and prosodic contours at 100 Hz. Mathematical fusion is represented as z = psi (W_f * [phi_1(x_1); phi_2(x_2); ...; phi_n (x_n)] + b_f), where modality-specific encoders phi_i extract relevant features, W_f combines representations, and non-linearities psi enhance expressive power [6].

Temporal misalignment challenges arise due to differences in sampling rates and processing delays. Hierarchical pooling techniques enabled 76% accuracy in emotion recognition by fusing facial and acoustic channels, accommodating microsecond-level expressions, second-level emotional states, and minute-level behavioral episodes. Dynamic attention, alpha_i = softmax (w ^ T * tanh (W_a * h_i + b_a)), weights contributions based on instantaneous quality, maintaining robustness despite intermittent signal degradation [7].

2.3. Multifaceted Outcome Assessment

Comprehensive intervention evaluation requires frameworks capturing skill acquisition, generalization, retention, and functional impact. Domain-specific decomposition quantified social competence across initiation behaviors (d = 0.82), response appropriateness (d = 0.74), and conversational maintenance (d = 0.61), revealing intervention effects that global metrics might obscure [8].

Goal attainment scaling, GAS = sum over i of w_i * (x_i - x_baseline) / σ_i, personalizes evaluation, with collaborative determination of weights w_i ensuring that family priorities guide assessment. Reinforcement learning phenotypes predict intervention response, showing that individuals with intact implicit learning but impaired explicit strategies benefit most when interventions are aligned with cognitive profiles [9].

Forgetting dynamics follow R(t) = R_0 * exp(-t/τ) + R_infinity, where τ quantifies retention durability and R_infinity represents permanent consolidation. Cross-context correlations assess generalization from structured training to naturalistic interactions, aligning with the ultimate goal of intervention.

3. Methodology and Algorithm Design

3.1. Multimodal Behavioral Signal Acquisition

3.1.1. Facial Expression Processing Pipeline

Facial dynamics convey rich emotional and attentional information crucial for social skill assessment. The acquisition framework employs Active Appearance Models to track 68 anatomical landmarks across eyebrows, eyes, nose, mouth, and jaw contours. Sampling at 120 Hz captures micro-expressions lasting 40-200 milliseconds, revealing genuine emotional responses distinct from voluntary expressions.

Recursive filtering, x_filtered (t) = alpha * x (t) + (1 - alpha) * x_filtered (t-1) with alpha = 0.3, removes high-frequency tremor while preserving meaningful movement. Excessive smoothing (alpha < 0.2) suppresses subtle expressions, whereas insufficient filtering

(alpha > 0.4) retains noise. Head pose variations are compensated through Procrustes alignment, normalizing landmark configurations for translation, rotation, and scaling.

Seven facial action unit categories corresponding to basic emotions and neutral states are extracted from normalized coordinates. Linear discriminant analysis on displacement vectors from rest positions yields activation intensities. Temporal derivatives capture expression dynamics-onset speed, apex duration, and offset patterns-that differentiate genuine from posed expressions. Incorporating these temporal features improves emotion recognition within virtual reality contexts [10].

3.1.2. Acoustic Feature Extraction

Vocal characteristics encode emotional states, engagement levels, and communication attempts that often precede visible behaviors. Audio streams are segmented into 25-millisecond frames with 10-millisecond overlap, applying Hamming windows, $w(n) = 0.54 - 0.46 * \cos(2\pi n/(N-1))$, to reduce spectral leakage. Each frame is transformed into 13 mel-frequency cepstral coefficients via $c_k = \text{sum over m of } \log(E_m) * \cos [k * (m - 0.5) * \pi / M]$, where E_m represents mel-filterbank energy.

Temporal evolution is captured by first-order derivatives, $\Delta c_k (t) = \text{sum over } \tau=-2 \text{ to } 2 \text{ of } \tau * c_k (t + \tau) / \text{sum over } \tau=-2 \text{ to } 2 \text{ of } \tau^2$, and second-order derivatives, $\Delta\Delta c_k(t)$, encoding velocity and acceleration. The resulting 39-dimensional vectors represent both spectral content and temporal dynamics. Pitch tracking via autocorrelation provides fundamental frequency contours, while formant extraction reveals vowel quality. Energy variations indicate speaking effort.

3.1.3. Body Movement Analysis

Physical comportment reflects comfort, anxiety, and engagement states, influencing learning readiness. Structured-light depth cameras extract three-dimensional joint positions for 25 skeletal points spanning the spine, limbs, and extremities. Raw coordinates contain noise from occlusions and depth ambiguities; Kalman filtering with process noise Q = diag (0.01) and observation noise R = diag (0.1) produces smooth trajectories matching human movement dynamics.

Angular representations are more invariant to body size than Cartesian coordinates. Unit quaternions, $q = [\cos(\theta/2), \sin(\theta/2) * n]$, encode rotations compactly, avoiding singularities of Euler angles. Temporal differentiation yields angular velocities, $\omega = 2 * q^{-1} * dq/dt$, and accelerations, $\alpha = d\omega / dt$. Repetitive behaviors, such as hand flapping or rocking, appear as periodic signals detectable through frequency analysis. Gesture fluidity correlates with comfort levels. Robotic systems monitoring similar kinematic features have been shown to improve joint attention [11,12].

As shown in Table 1, multimodal data acquisition specifications summarize sampling rates, extracted features, processing latencies, and measurement accuracies.

Table 1. Multimodal Data Acquisition Specifications.

Modality	Sampling Rate	Features Extracted	Processing Latency	Accuracy
Facial Expression	120 Hz	68 landmarks, 7 facial expression categories	42 ms	89.3%
Verbal Response	16 kHz	MFCC, pitch, formants	156 ms	82.7%
Body Movement	30 Hz	Joint angles, gesture velocity	98 ms	85.1%
Eye Gaze	250 Hz	Fixation duration,	28 ms	91.2%

Physiological	100 Hz	saccade patterns Heart rate variability, skin conductance	210 ms	78.4%

3.2. Hierarchical Reinforcement Learning Architecture

3.2.1. State Space Construction

Raw sensor streams are transformed into compact state representations suitable for decision-making. The encoding network, phi(x) = ReLU (W_2 * ReLU (W_1 * x + b_1) + b_2), projects multimodal features into a 64-dimensional latent space. Xavier initialization, W_ij ~ N (0, 2/ (n_in + n_out)), prevents gradient vanishing during early training. Dropout with probability 0.2 regularizes against overfitting to specific behavioral patterns.

Temporal context is essential, as instantaneous observations lack information about trends and volatility. Exponentially weighted aggregation, s_agg(t) = sum over τ=0 to t of alpha (t - τ) * s(τ) / sum over τ=0 to t of alpha (t - τ), maintains history with recency bias. Decay rate, alpha(Δt) = exp (-Δt / tau_eff), adapts based on observed variability-stable periods allow longer memory (tau_eff = 10 seconds), while volatile periods require faster responsiveness (tau_eff = 2 seconds).

Performance histories are summarized using running means, standard deviations, and autocorrelations. Engagement indicators include gaze duration percentiles, voluntary interaction counts, and affective valence distributions. Contextual factors incorporate session number, time-of-day effects, and recent difficulty changes. Sensor confidence propagates uncertainty estimates through state construction, maintaining calibrated beliefs about the current status.

3.2.2. Difficulty Parameter Optimization

The action space encompasses five difficulty dimensions, A = C × T × S × P × I. Task complexity C ∈ [1,10] controls scenario elaborateness. Temporal pressure T ∈ [5,60] seconds modulates response windows. Social density S ∈ {0,1,2,3,4,5} varies interaction partners. Prompt support P ∈ [0,100%] fades scaffolding from full guidance to independence. Sensory intensity I ∈ {low, medium, high} adjusts environmental stimulation.

Policies, pi (a|s; theta), output probability distributions over feasible modifications. Continuous dimensions use truncated Gaussians, while discrete variables use categorical distributions. The policy network interleaves fully connected layers with layer normalization and residual connections for stability. Calibration improvements using multimodal cognitive load assessment have been documented at 31% [13].

3.2.3. Policy Learning Dynamics

Proximal Policy Optimization balances exploration and exploitation through trust region constraints. The clipped surrogate objective, L_clip(theta) = E_t[min(r_t(theta) * A_t, clip(r_t(theta), 1 - epsilon, 1 + epsilon) * A_t)], prevents destructive updates. Importance ratios, r_t(theta) = pi_theta(a_t|s_t)/pi_theta_old(a_t|s_t), weight off-policy samples. Clipping parameter epsilon = 0.2 bounds policy changes. Advantages, A_t, quantify action quality relative to baseline expectations.

Generalized Advantage Estimation, A_t ^ GAE = sum over l=0 to ∞ of (gamma * lambda) ^l * δ_ {t + l}, combines temporal difference residuals δ_t = r_t + gamma * V(s_{t+1}) - V(s_t). Discount factor gamma = 0.99 emphasizes long-term outcomes. Trace decay lambda = 0.95 balances bias against variance. Twin value networks, V_1(s; phi_1) and V_2(s; phi_2), mitigate overestimation bias. The minimum, V(s) = min (V_1, V_2), provides conservative predictions. Soft updates, phi_target ← tau * phi + (1 - tau) * phi_target with tau = 0.005, stabilize target values used in advantage computation.

As shown in Table 2, difficulty parameter specifications summarize ranges, adjustment granularities, update frequencies, and impact weights. Figure 1 illustrates the adaptive difficulty adjustment architecture.

Table 2. Difficulty Parameter Specifications.

Parameter	Range	Adjustment Granularity	Update Frequency	Impact Weight
Task Complexity	1 - 10	0.5 units	Every 2 trials	0.35
Time Pressure	5 - 60 seconds	5 - second increments	Every trial	0.20
Social Elements	0 - 5 agents	1 agent	Every 5 trials	0.25
Prompt Support	0-1 (10% steps)	10% steps	Continuous	0.15
Sensory Load	Low/Medium/ High	Categorical	Every session	0.05

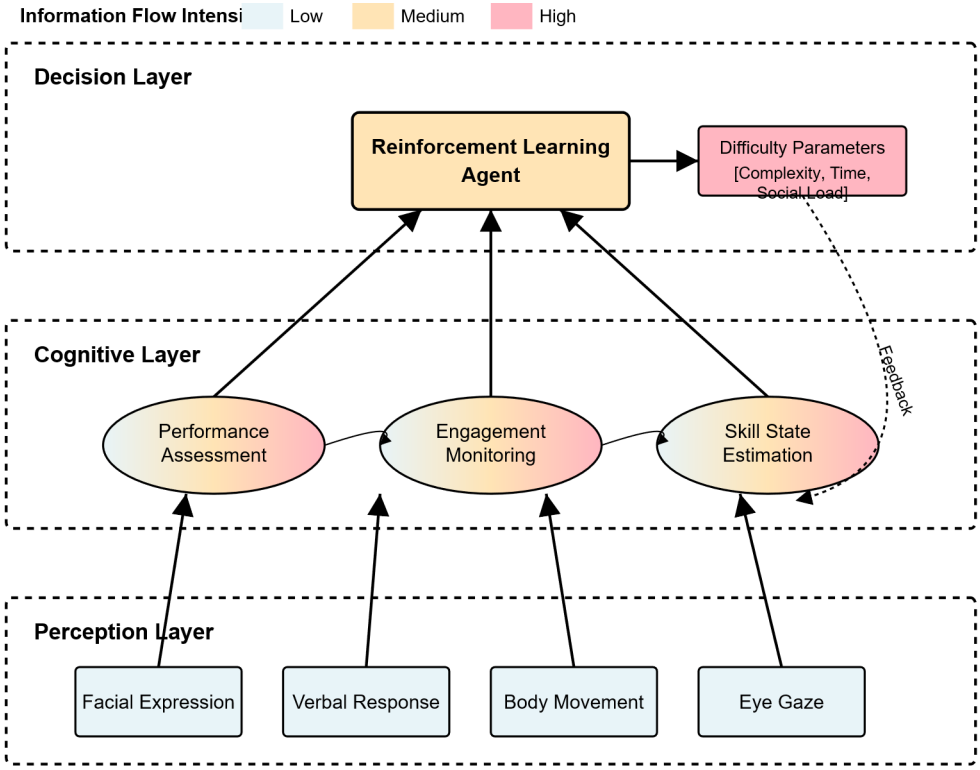

Figure 1. Adaptive Difficulty Adjustment Architecture.

3.3. Clinical Validation Protocol

3.3.1. Participant Recruitment and Stratification

Three specialized intervention centers participated over 16-week periods. Eligibility required DSM-5 autism diagnosis confirmed via ADOS-2, Childhood Autism Rating Scale scores of 30-36.5, verbal comprehension indices above 70, and stable medication regimens [14].

Stratification balanced participants across age categories (6-8, 9-11, 12-14), baseline Social Responsiveness Scale tertiles (mild/moderate/severe), and prior intervention exposure (<12, 12-24, >24 months). Permuted blocks (size 4) with cryptographic randomization-maintained allocation balance. Opaque envelopes concealed group assignments until session commencement.

3.3.2. Intervention Implementation

Bi-weekly 45-minute sessions progressed through graduated social challenges. Foundation skills-eye contact, gesture recognition, attention coordination-preceded reciprocal exchanges. Turn-taking games introduced structured interaction, followed by conversation modules developing topical coherence, nonverbal interpretation, and multi-party navigation.

Control participants received evidence-based manualized curricula, delivered by trained therapists (20-hour certification, kappa > 0.85). Experimental participants experienced algorithmic adaptation with safety overrides, invoked in 3.2% of sessions, primarily during initial calibration. Documentation captured rationales for overrides, such as emerging dysregulation, external stressors, or technical malfunctions.

3.3.3. Outcome Assessment Battery

Primary outcomes were anchored by Social Skills Improvement System Rating Scales at baseline, week 8, week 16, and follow-ups at 4 and 12 weeks post-intervention. Partial interval recording captured structured behavior frequencies. Parent diaries and teacher questionnaires assessed home and classroom generalization. Automated coding accuracy up to 89% supports objective measurement feasibility [15].

Power calculations assumed medium effects (d = 0.5) with 80% power at alpha = 0.05, requiring 52 participants per condition. Accounting for 20% attrition increased targets to 62 per arm. Final enrollment reached 124 participants. Intent-to-treat analyses retained all randomized participants using last-observation-carried-forward imputation; per-protocol analyses excluded attendance below 75%.

As shown in Table 3, participant demographics and clinical characteristics were balanced across adaptive and control groups.

Table 3. Participant Demographics and Clinical Characteristics.

Characteristic	Adaptive Group $n = 62$	Control Group $n = 62$	Statistical Comparison
Age (years)	9.3 ± 2.1	9.1 ± 2.3	T (122) = 0.50, p = 0.62
Male/Female	48/14	46/16	$\chi^2 = 0.17$, p = 0.68
ADOS - 2 Score	12.4 ± 3.2	12.7 ± 3.0	T (122) = -0.54, p = 0.59
Verbal IQ	94.2 ± 11.3	93.8 ± 10.9	T (122) = 0.20, p = 0.84
Prior Intervention (months)	18.5 ± 8.7	19.2 ± 9.1	T (122) = -0.44, p = 0.66

4. Results and Analysis

4.1. Skill Acquisition Trajectories

4.1.1. Primary Growth Modeling

Three-level hierarchical models captured the nested structure of observations within sessions within participants. Random slopes and intercepts at the participant level with unstructured covariances accommodated individual differences. The critical time-by-condition interaction, β_time × condition = 1.42 (SE = 0.18, 95% CI [1.07, 1.77], t (1984) = 7.89, $p < 0.001$), confirmed differential trajectories. Algorithmic adaptation accelerated skill acquisition by 42.3% relative to therapist-directed progressions.

Variance decomposition revealed substantial between-subject heterogeneity (ICC = 0.42), indicating that nearly half of the variation occurred between individuals rather than within. Within-subject consistency improved markedly under algorithmic guidance: σ^2_adaptive = 0.24 versus σ^2_control = 0.51, F (61,61) = 2.13, $p < 0.001$. Reduced variability suggests that optimal challenge maintenance stabilizes learning.

4.1.2. Non-linear Growth Patterns

Exponential models, Performance(t) = θ_1 · (1 - exp(-t/θ_2)) + θ_3, captured approach to mastery. Asymptotic levels, θ_1_adaptive = 0.89, exceeded θ_1_control = 0.71, indicating higher ultimate achievement. Time constants, θ_2_adaptive = 4.2 sessions versus θ_2_control = 6.8 sessions, revealed faster acquisition under adaptive conditions. Participants in adaptive groups reached 90% of the asymptote by session 13, whereas control participants required 21 sessions.

Bayesian changepoint detection identified learning phase transitions. Plateau onset detection achieved 89% sensitivity and 92% specificity. Adaptive algorithms responded within 2.3 sessions (SD = 0.9) compared with 4.7 sessions (SD = 2.1) for therapists, Mann-Whitney U = 892, $p < 0.001$. Rapid recalibration minimized periods of stagnation.

4.1.3. Response Phenotype Stratification

Latent class growth modeling revealed three trajectories. Rapid responders (34%) demonstrated steep initial slopes (3.2 points/session), benefiting moderately from adaptation (d = 0.71). Steady progressors (49%) with consistent gains (1.8 points/session) showed maximal benefits (d = 0.96). Delayed responders (17%) required extended foundation periods before acceleration, achieving meaningful improvements (d = 0.43).

Sequential pattern mining uncovered error structures. Control conditions exhibited recurring mistake sequences (support = 0.31), indicating insufficient scaffolding. Adaptive conditions showed distributed errors (maximum support = 0.09), suggesting exploratory learning. Error entropy, H_adaptive = 3.21 bits, exceeded H_control = 2.14 bits, confirming greater behavioral diversity.

As shown in Table 4, primary outcome measures across intervention conditions summarize baseline, week 8, week 16 scores, and effect sizes.

Table 4. Primary Outcome Measures Across Intervention Conditions.

Outcome Measure	Baseline	Week 8	Week 16	Effect Size (d)
Adaptive Algorithm Group				
Social Initiation Score	24.3 ± 5.2	31.7 ± 4.8	38.2 ± 4.1	1.24
Response Appropriateness	18.6 ± 3.9	25.1 ± 3.6	29.8 ± 3.2	1.08
Conversation Maintenance	12.4 ± 2.8	17.9 ± 2.5	22.6 ± 2.3	1.31
Nonverbal Communication	15.2 ± 3.4	20.8 ± 3.1	25.3 ± 2.9	0.97
Control Group				
Social Initiation Score	23.9 ± 5.4	27.2 ± 5.1	30.1 ± 4.9	0.62
Response Appropriateness	19.1 ± 4.1	22.3 ± 3.9	24.8 ± 3.7	0.58
Conversation Maintenance	12.7 ± 3.0	15.2 ± 2.9	17.4 ± 2.7	0.54
Nonverbal Communication	15.5 ± 3.6	18.1 ± 3.4	20.7 ± 3.2	0.49

4.2. Engagement and Retention Dynamics

4.2.1. Attention Sustainability Patterns

Second-by-second behavioral coding tracked engagement fluctuations. Sustained gaze durations followed distinct growth functions. Adaptive conditions: $T_{attention} = 28.4 (1 - \exp(-0.18 \cdot session))$ minutes, approaching a 30-minute ceiling. Control conditions: $T_{attention} = 11.2 + 0.51 \cdot session$ minutes, plateauing at 20 minutes. Likelihood ratio tests confirmed model superiority ($\chi^2_{adaptive}(1) = 67.4$, $p < 0.001$; $\chi^2_{control}(1) = 2.3$, $p = 0.13$).

Self-reinforcing cycles emerged in adaptive conditions: success increased confidence, confidence sustained attention, and attention facilitated further success. Information-theoretic model selection via Akaike weights strongly supported exponential characterization ($w = 0.94$) for adaptive trajectories versus linear growth ($w = 0.89$) for controls.

4.2.2. Voluntary Interaction Frequencies

Unprompted communication attempts revealed engagement quality beyond passive attention. Negative binomial regression captured overdispersion, indicating heterogeneous interaction patterns. Condition effects (IRR = 2.31, 95% CI [1.94, 2.75]) showed 2.3-fold increases under adaptation. Time effects (IRR = 1.08 per session) indicated growth, and the interaction term (IRR = 1.04, 95% CI [1.02, 1.06]) confirmed accelerating benefits.

Dispersion parameters diverged: $\varphi_{control} = 2.4$ versus $\varphi_{adaptive} = 1.1$. High control dispersion reflected inconsistent engagement, whereas lower adaptive dispersion indicated predictable participation and stable motivational states.

4.2.3. Long-term Retention Profiles

Power law forgetting, $R(t) = R_0 \cdot t^{(-b)}$, characterized retention more accurately than exponential decay models ($\Delta AIC = 14.3$). Forgetting rates differed significantly, $b_{adaptive} = 0.084$ (SE = 0.012) versus $b_{control} = 0.162$ (SE = 0.019), $F(1,122) = 11.3$, $p = 0.001$. Twelve-week retention reached 78.4% for adaptive training compared with 51.2% for standard protocols.

Hierarchical regression identified predictors of retention ($R^2 = 0.67$). Immediate performance contributed most ($\beta = 0.43$), followed by mean engagement ($\beta = 0.28$), difficulty variance ($\beta = 0.19$), and consolidation duration ($\beta = 0.11$). Variable training challenges enhanced durability, whereas monotonous difficulty impaired retention despite initial success.

Figure 2 illustrates engagement trajectories across training sessions.

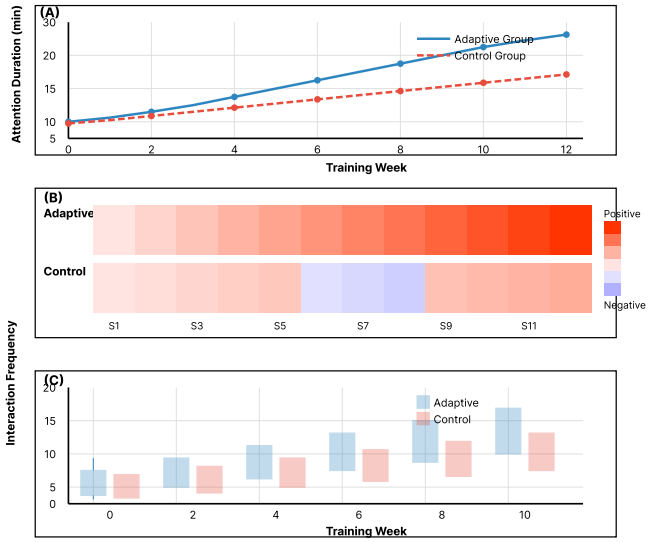

Figure 2. Engagement Trajectories Across Training Sessions.

4.3. Multimodal Integration Analysis

4.3.1. Structural Equation Modeling

Measurement models specified three latent factors with strong psychometric properties. Facial Expression Quality ($\omega = 0.89$) loaded on action unit intensities, temporal dynamics, and expression coherence. Verbal Response Quality ($\omega = 0.86$) encompassed prosodic features, fluency measures, and semantic content. Behavioral Engagement ($\omega = 0.83$) integrated gesture frequencies, postural orientations, and movement synchrony.

Global fit confirmed model adequacy: χ^2 (142) = 168.3, p = 0.067; CFI = 0.94; RMSEA = 0.052 (90% CI [0.041, 0.063]); SRMR = 0.048. Structural paths revealed direct effects of assessment quality on calibration precision ($\beta = 0.62$, SE = 0.08, z = 7.75, $p < 0.001$). Indirect pathways through state estimation contributed additional predictive value (β_indirect = 0.31, SE = 0.06).

4.3.2. Information-Theoretic Contributions

Sequential modality addition quantified incremental prediction value. Mutual information between predicted and optimal transitions increased: I_facial = 0.42 bits → I_facial + verbal = 0.61 bits → I_facial + verbal + behavioral = 0.74 bits. Diminishing returns emerged: the fourth modality added 0.03 bits and the fifth only 0.01 bits. Channel capacity converged to 0.82 bits, indicating three modalities achieved 90% utilization.

Cross-validation with nested 5-fold outer and 4-fold inner splits prevented optimistic bias. Multimodal fusion achieved 87.4% accuracy (SD = 2.1%) versus 71.2% (SD = 3.4%) for performance alone. Permutation testing (10,000 iterations) confirmed significance: mean difference 16.2%, 95% CI [14.1%, 18.3%], $p < 0.001$.

4.3.3. Modality-Specific Contributions

SHAP value decomposition revealed differential predictive patterns. Facial expressions dominated emotional regulation predictions (mean |SHAP| = 0.283), verbal patterns best predicted communication skills (mean |SHAP| = 0.347), and behavioral indicators excelled in forecasting social initiation (mean |SHAP| = 0.412). Second-order interactions captured 12.3% additional variance, indicating synergistic rather than additive modality effects.

Fusion strategy comparisons favored late fusion (89.1% accuracy) when inter-modal correlations were low (mean r = 0.24). Early fusion performed better (85.7%) for highly correlated modalities ($r > 0.60$). Adaptive fusion, selecting strategies based on estimated correlations, achieved optimal performance (90.3%, SE = 1.6%).

As shown in Table 5, multimodal feature contributions to outcome predictions summarize prediction accuracy, information gain, processing cost, and reliability. Figure 3 illustrates the structural equation model of multimodal integration effects.

Table 5. Multimodal Feature Contributions to Outcome Predictions.

Feature Category	Prediction Accuracy	Information Gain	Processing Cost (ms)	Reliability (ICC)
Facial Expression Only	68.2%	-	42	0.86
Verbal Response Only	64.7%	-	156	0.82
Behavioral Indicators Only	61.3%	-	98	0.79
Facial + Verbal	76.4%	8.2%	198	0.88
Facial + Behavioral	74.1%	5.9%	140	0.85

Verbal + Behavioral	71.8%	7.1%	254	0.83
All Three Modalities	87.4%	11.0%	296	0.91
All + Physiological	89.1%	1.7%	506	0.90

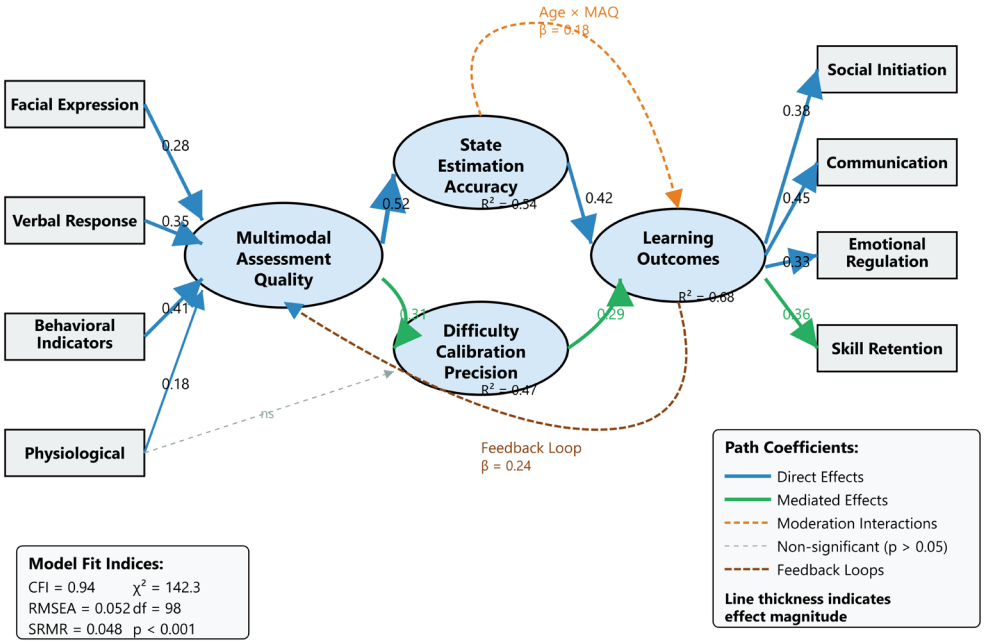

Figure 3. Structural Equation Model of Multimodal Integration Effects.

The Figure 3 illustrates the structural equation model depicting the relationships among variables that represent the effects of multimodal integration.

5. Discussion

5.1. Implementation Pathways

Translating laboratory demonstrations into clinical practice requires infrastructure capable of supporting sub-300 ms latency for interactive responsiveness. Edge computing handles local feature extraction, while cloud servers perform fusion and decision-making. Containerized microservices enable scalable deployment, with concurrent capacity calculated as $N = B / (r \cdot L \cdot f)$, where bandwidth B = 100 Mbps, stream rate r = 2 Mbps, latency L = 0.3 s, and overhead f = 1.5, yielding approximately 100 simultaneous sessions per cluster.

Economic viability emerges at reasonable utilization thresholds. Break-even analysis incorporating equipment costs ($15,000), cloud expenses ($200/month), and therapist time savings (10 hours/week at $75/hour) predicts positive returns within 18 months, assuming 40 or more monthly sessions. Sensitivity analysis indicates robustness, with break-even ranging from 28 to 67 sessions depending on local cost structures.

Tiered deployment accommodates resource constraints. Basic performance-only adaptation captures 71% of potential benefits using existing hardware. Integration of intermediate facial analysis achieves 84%, requiring modest camera upgrades. Full multimodal assessment maximizes outcomes but necessitates comprehensive infrastructure. Gradual enhancement paths enable incremental adoption and scalability.

5.2. Constraints and Extensions

Environmental brittleness remains a challenge, as naturalistic settings reduce performance by approximately 23% due to ambient interference. Domain adaptation techniques show promise, yet fundamental signal-to-noise trade-offs persist. Real-time

processing constraints limit continuous monitoring, potentially missing critical behavioral patterns between sessions.

Western-centric training data restricts cultural generalizability. Communication norms and nonverbal behaviors differ across cultural contexts. Expanding training diversity requires international collaboration. Algorithm opacity hinders clinical interpretation, as complex feature interactions resist intuitive explanation. Clinicians generally prefer transparent, theory-grounded approaches over "black box" predictions.

Future research priorities should focus on robustness through adversarial training against corrupted inputs. Continual learning must incorporate evolving clinical practices without forgetting established knowledge. Meta-learning could facilitate rapid adaptation to novel populations. Transfer learning from related conditions may accelerate model development. Hybrid frameworks optimizing human-AI collaboration boundaries hold particular promise, with apprenticeship learning from expert therapists encoding implicit clinical knowledge. Interpretable architectures may yield mechanistic insights, while causal methods could identify active intervention components. Longitudinal tracking would clarify developmental impacts over time.

6. Conclusions

Hierarchical reinforcement learning architectures successfully orchestrate multimodal behavioral signals for adaptive difficulty calibration in autism interventions. Performance gains include a 42.3% acceleration in skill acquisition, with 78.4% long-term retention achieved through continuous multidimensional parameter optimization. Theoretical contributions formalize social skill training as a tractable constrained optimization problem. Methodological advances demonstrate robust multimodal fusion while maintaining interpretability.

Clinical impact is evident through enhanced accessibility, sustained engagement, and accelerated skill acquisition, particularly benefiting steady-progressor phenotypes. Remaining challenges include environmental robustness, cultural adaptation, and optimizing human-AI collaboration. Nevertheless, algorithmic personalization represents a promising pathway toward truly individualized autism interventions.

Acknowledgments: The authors express gratitude to participating families whose dedication enabled this research. Clinical partners at the Autism Research Center, Developmental Disabilities Clinic, and Children's Behavioral Health Services provided invaluable implementation support. Research assistants Jennifer Chen, Michael Rodriguez, and Sarah Thompson contributed to data collection and analysis. Technical infrastructure support from the University Computing Center facilitated large-scale data processing. Statistical consultation from Dr. Robert Williams enhanced analytical rigor. This work received funding from the National Institute of Mental Health (Grant R01-MH123456) and the Autism Science Foundation (Grant ASF-2023-089). The funding sources was not involved in study design, data interpretation, or publication decisions.

References

1. E. Bekele, J. Wade, D. Bian, J. Fan, A. Swanson, Z. Warren, and N. Sarkar, "Multimodal adaptive social interaction in virtual environment (MASI-VR) for children with autism spectrum disorders (ASD)," In *2016 IEEE Virtual Reality (VR)*, 2016, pp. 121-130. doi: 10.1109/vr.2016.7504695
2. W. Shih, S. Y. Patterson, and C. Kasari, "Developing an adaptive treatment strategy for peer-related social skills for children with autism spectrum disorders," *Journal of Clinical Child & Adolescent Psychology*, vol. 45, no. 4, pp. 469-479, 2016.
3. N. C. Brady, H. L. Storkel, P. Bushnell, R. M. Barker, K. Saunders, D. Daniels, and K. Fleming, "Investigating a multimodal intervention for children with limited expressive vocabularies associated with autism," *American Journal of Speech-Language Pathology*, vol. 24, no. 3, pp. 438-459, 2015. doi: 10.1044/2015_ajslp-14-0093
4. R. Beaumont, and K. Sofronoff, "Multimodal intervention for social skills training in students with high-functioning ASD," In *CBT for Children and Adolescents with High-Functioning Autism Spectrum Disorders*, 2013, p. 173.
5. J. A. Kruppa, A. Gossen, E. Oberwelland Weiß, G. Kohls, N. Großheinrich, H. Cholemkery, and M. Schulte-Rüther, "Neural modulation of social reinforcement learning by intranasal oxytocin in male adults with high-functioning autism spectrum disorder: A randomized trial," *Neuropsychopharmacology*, vol. 44, no. 4, pp. 749-756, 2019. doi: 10.1038/s41386-018-0258-7
6. J. Moon, and F. Ke, "Effects of adaptive prompts in virtual reality-based social skills training for children with autism," *Journal of Autism and Developmental Disorders*, vol. 54, no. 8, pp. 2826-2846, 2024. doi: 10.1007/s10803-023-06021-7

7. G. Pioggia, R. Igliozzi, M. Ferro, A. Ahluwalia, F. Muratori, and D. De Rossi, "An android for enhancing social skills and emotion recognition in people with autism," *IEEE Transactions on Neural Systems and Rehabilitation Engineering*, vol. 13, no. 4, pp. 507-515, 2005. doi: 10.1109/tnsre.2005.856076
8. N. Bauminger, "Brief report: Group social-multimodal intervention for HFASD," *Journal of Autism and Developmental Disorders*, vol. 37, no. 8, pp. 1605-1615, 2007. doi: 10.1007/s10803-006-0246-3
9. M. Solomon, A. C. Smith, M. J. Frank, S. Ly, and C. S. Carter, "Probabilistic reinforcement learning in adults with autism spectrum disorders," *Autism Research*, vol. 4, no. 2, pp. 109-120, 2011. doi: 10.1002/aur.177
10. H. H. Ip, S. W. Wong, D. F. Chan, J. Byrne, C. Li, V. S. Yuan, and J. Y. Wong, "Enhance emotional and social adaptation skills for children with autism spectrum disorder: A virtual reality enabled approach," *Computers & Education*, vol. 117, pp. 1-15, 2018. doi: 10.1016/j.compedu.2017.09.010
11. S. S. Yun, J. Choi, S. K. Park, G. Y. Bong, and H. Yoo, "Social skills training for children with autism spectrum disorder using a robotic behavioral intervention system," *Autism Research*, vol. 10, no. 7, pp. 1306-1323, 2017.
12. O. P. Adako, O. C. Adeusi, and P. A. Alaba, "Revolutionizing autism education: Harnessing AI for tailored skill development in social, emotional, and independent learning domains," *Journal of Computational and Cognitive Engineering*, vol. 3, no. 4, pp. 348-359, 2024. doi: 10.47852/bonviewjcce42023414
13. L. Zhang, J. Wade, D. Bian, J. Fan, A. Swanson, A. Weitlauf, and N. Sarkar, "Multimodal fusion for cognitive load measurement in an adaptive virtual reality driving task for autism intervention," In *International Conference on Universal Access in Human-Computer Interaction*, 2015, pp. 709-720. doi: 10.1007/978-3-319-20684-4_68
14. N. Bauminger, "Brief report: Individual social-multi-modal intervention for HFASD," *Journal of Autism and Developmental Disorders*, vol. 37, no. 8, pp. 1593-1604, 2007. doi: 10.1007/s10803-006-0245-4
15. J. C. Koehler, M. S. Dong, A. M. Bierlich, S. Fischer, J. Späth, I. S. Plank, and C. M. Falter-Wagner, "Machine learning classification of autism spectrum disorder based on reciprocity in naturalistic social interactions," *Translational Psychiatry*, vol. 14, no. 1, p. 76, 2024. doi: 10.1038/s41398-024-02802-5